Behavior of ortho-positronium in low-temperature nitrogen

T. Kawaratani
Laboratory of Nuclear Radiation, Institute for Chemical Research, Kyoto University, Sakyo-Ku, Kyoto 606, Japan

Y. Nakayama
Department of Physics, Ritsumeikan University, Kita-ku, Kyoto 603, Japan

T. Mizogawa
The Institute of Physical and Chemical Research, Wako, Saitama 351-01, Japan

(Received 3 June 1987)

Ortho-positronium (*o*-Ps) annihilation rates have been measured in N_2 at temperatures in the range 100–170 K. Deviations from the annihilation rates expected for free *o*-Ps are observed, and are analyzed by current models where applicable. A density-functional calculation using an optical potential indicates that the large deviations at higher densities are attributable to the formation of *o*-Ps–induced bubbles, and the *o*-Ps–N_2 scattering length is about 0.8 Å. Analysis by the density-fluctuation model suggests, on the other hand, that the relatively small deviations observed at lower densities are due to the existing density fluctuations. A semiclassical approach is also attempted to apply to problems of the density of states and the annihilation rates of ortho-positronium in gases.

I. INTRODUCTION

At sufficiently low densities the annihilation rate of ortho-positronium (*o*-Ps) in nonpolar gases is known to increase linearly with density. However, deviation of the annihilation rate from such linear dependence is observed in some regions of density and temperature. The deviation usually appears at high density and comparably low temperature to the critical temperature of the gas, and the deviation is downward from the linear dependence.

One idea to interpret this behavior is an *o*-Ps–induced bubble.[1] Due to the dominant repulsive interaction between *o*-Ps and a gas atom (molecule), *o*-Ps creates a bubble around itself and then becomes trapped in the bubble. This truly occurs when the binding energy of *o*-Ps in the bubble exceeds the work necessary to create the bubble. An *o*-Ps–induced bubble is quite analogous to an electron-induced bubble,[2–4] which contains the electron and gives rise to a decrease of magnitude in the electron's mobility. In a theoretical approach, the *o*-Ps bubble is regarded as a three-dimensional square-well potential in the simplest way,[5–8] or analyzed by calculating the density distribution around *o*-Ps self-consistently.[9–12] The former, which is called the "square-well model," reasonably represents this object in the limit of very strong binding to the bubble relative to the extended state.[10] The latter, the density-functional method, is a more sophisticated approach which removes the defect in the former that postulates a bubble-density profile *a priori*. For the annihilation rate of a free positron, this method has succeeded in explaining the nonlinear behavior which is related to the positron-induced cluster phenomenon in He,[13,14] Ar,[15] and N_2.[16] It has also predicted the stable region for the electron bubble and its density profile in He.[9,17–20] As for the *o*-Ps bubble, this method has been applied to He,[9–11] Ne,[11] and Ar,[12] and has shown that there exist stable bubbles in these gases and that the deviations of the *o*-Ps annihilation rate observed in certain temperature and density ranges can be understood in terms of the *o*-Ps bubble. However, these same calculations have shown disagreement with the experimental results mainly in the onset region of deviation and the next region of higher density.

Another idea for explaining the nonlinear behavior of the *o*-Ps annihilation rate comes from density fluctuations in gases. In this picture, it is considered that *o*-Ps does not actively dig a cavity around itself, but rather passively interacts with the existing density fluctuations without influencing a local structure of the gas around itself. In CH_4,[21] C_2H_6,[22,23] CO_2,[24] N_2,[25] and Ar,[12] correlations have been found between the deviations of the *o*-Ps annihilation rate and gas quantities related to the density fluctuations. The so-called density-fluctuation model,[21] which treats the effect of the density fluctuations on the *o*-Ps annihilation rate from a classical thermodynamic point of view, has explained the deviation especially in the onset and next-higher-density regions in several gases. On the other hand, the role of the density fluctuation in the *o*-Ps behavior is discussed from the quantum-mechanical point of view, too. Such an approach, however, gives rise to a difficult problem characteristically associated with the theory for states of a light particle in disordered materials. A few studies[26–29] along this line have been done for an excess electron and for *o*-Ps. Especially for the excess-electron behavior, the approach of Eggarter and Cohen[26,27] employing semiclassical counting[30] to determine the density of states of the electron and a percolation theory to deduce the degree of localization of the states has explained the rapid and extreme decrease of the mobility in low-temperature He. This success provides one possibility of solving the behavior of

the o-Ps annihilation rate in the region where the discrepancy exists between the density-functional calculation and the experimental results, but there is no quantitative study giving specific predictions comparable with the experimental data.

The o-Ps annihilation in gases is practically the only method that brings us knowledge of the o-Ps–gas interaction. Moreover, this is important for studying the behavior of the quantum particle in fluids, since the annihilation process reflects the local structure of the fluid around the particle more directly than a quantity such as the mobility. Although preceding investigations have revealed interesting features of the o-Ps behavior in gases, some problems remain to be solved.

In order to better understand the behavior of o-Ps in gases, we report in this paper experimental results of the o-Ps annihilation rates in N_2 as a function of density, pressure, and temperature of the gas. We further present detailed comparisons with the current models where applicable. The experimental results show a linear relation between the o-Ps annihilation rate and the gas pressure over wide temperature and pressure ranges, and they show correlations between the deviations observed and some quantities dependent on the density fluctuations of N_2. The deviations observed in the onset region and the next region of higher density are consistent with the prediction of the density-fluctuation model. On the other hand, the density-functional calculation indicates that the o-Ps bubble exists stably in the region of higher densities at the temperature near the critical temperature where the density-fluctuation model breaks down. The semiclassical approach based on the Eggarter-Cohen model does not explain the behavior of the o-Ps annihilation rate in N_2, although it gives reasonable results for the o-Ps in low-temperature He.

II. EXPERIMENTAL PROCEDURE

A. Apparatus

The gas chamber used was machined from an oxygen-free high-conductivity (OFHC) copper rod, and its internal surface was electroplated with gold to enhance the fraction of positrons stopping in the gas. Its dimension is 28 mm in internal diameter and 70 mm in active length. A ^{22}Na positron source (~ 7 μCi) deposited on a thick gold foil was wrapped by a thin Mylar film and held near the chamber wall. The chamber wall is about 4 mm thick, sufficient to withstand a pressure of over 100 atm and still provide good heat conduction. A lead-plated annealed copper-ring gasket was used for sealing the chamber. As positron lifetime parameters are sensitive to impurities in the sample gas, careful gas handling is required. Gas lines were constructed of stainless-steal tubing (6.34 mm in outer diameter). The system was cleaned with high-purity trichloroethylene before assembly, and then an evacuating and gas flushing procedure was performed many times. The chamber was held in a sealed copper cylinder immersed in liquid N_2 by a vacuum-insulated gas supply tube. A Pt resistance thermometer and a Au(+0.07% Fe)-chromel thermocouple were inserted into small holes drilled at the bottom part of the chamber. The temperature of the chamber was controlled by balancing the cooling produced by a low-pressure exchange gas with heating by a heater coil wound along the chamber. The heater power was supplied from an automatic temperature controller. The instability of the temperature was less than ± 0.1 K. The temperature of the chamber was measured by the Pt thermometer, which has been commercially calibrated. In order to check the manufacturer's calibration and estimate a temperature difference over the chamber, we compared the published vapor-pressure curve of liquid N_2 (Ref. 31) and Ar (Ref. 32) with measured vapor pressure in the chamber. The uncertainty in temperature determination, arising from the combined effects of temperature difference over the chamber and of errors in the calibration, is estimated to be less than ± 0.5 K. Commercially supplied high-purity-grade N_2 (minimum purity 99.9999%) was used for the sample gas. Gas pressures were measured by using precision Bourdon gauges. The accuracy of the measured pressure is better than 1% for all the data points above 2.4 atm and better than 2% for the other lower data points. The measured pressures were corrected for barometric fluctuations at low pressures. The density (D in amagats, 1 amagat $=2.69\times 10^{19}$ cm^{-3}) of N_2 gas was evaluated from measured pressure-temperature data by using a semiempirical equation of state given by Jacobsen *et al.*[31] The error in density estimation due to all causes is to be less than 3% for all the data at 100, 120, 150, and 170 K, and for data in the density regions $D \lesssim 100$ and $D \gtrsim 350$ at 130 K. For the data at 130 and 140 K outside the above regions it exceeds 3%, being 6% at 140 K at maximum, and especially in the vicinity of the critical points ($150 \lesssim D \lesssim 300$ at 130 K, $T_c = 126.2$ K and $D_c \simeq 250$ amagat) it becomes more than 10%.

Lifetime spectra have been measured by a system having the merit of a high counting rate similar to one developed by Coleman *et al.*[33] Detectors consisted of large fast plastic scintillators (12 cm in diameter by 10 cm high and 12 cm in diameter by 7.5 cm high for start and stop detectors, respectively) and photomultipliers (RCA 4522). The start and stop rates were approximately 7×10^3 and 2×10^4 s^{-1}, and the coincidence rate was about 6×10^2 s^{-1}. The time resolution was about 1.2 ns full width at half maximum (FWHM) for ^{60}Co.

A raw spectrum obtained from this system is deformed by random-coincidence events due to the high counting rate. Therefore, it was processed by the "signal-restoration method"[34] to deduce the restored ("true") spectrum before the usual nonlinear fitting analysis. The restored spectra excluding the prompt region were fitted by a simple exponential fitting program into two components as free fitting parameters when the free positron component was sufficiently separated from the prompt peak, or into one component when it overlapped with the prompt peak. The statistical accuracies of most results for the o-Ps annihilation rate are from below 1% to at most 2.5% at the lowest gas densities.

B. Results

Measurement of o-Ps annihilation rate $\lambda_{o\text{-Ps}}$ was carried out at 100, 120, 130, 140, 150, and 170 K, and at pressures in the ranges 1.5–7.7, 1.5–23.4, 1.6–75.5, 29.5–78.8, 3.9–73.4, and 3.0–76.7 atm, respectively. These pressure ranges correspond to the density ranges 4.2–25.5, 3.5–85.5, 3.4–428, 76.3–359, 7.3–250, and 4.8–170 amagat, respectively.

The o-Ps annihilation rate is represented as a sum of a vacuum annihilation rate λ_{vac} and a pickoff quenching rate λ_p. The former is constant independent of media; currently, for example, a value of $7.056\pm0.007\ \mu s^{-1}$ (Ref. 35) is presented experimentally and $7.0386\pm0.0002\ \mu s^{-1}$ (Ref. 36), theoretically. The pickoff rate varies widely reflecting a local electron density from molecules surrounding o-Ps. In many low-density gases λ_p increases linearly with increasing density, and then $\lambda_{o\text{-Ps}}$ is written in the form of

$$\lambda_{o\text{-Ps}}=\lambda_{\text{vac}}+4\pi r_0^2 cn\ {}^1Z_{\text{eff}} =\lambda_{\text{vac}}+4\pi r_0^2 cn_L\ {}^1Z_{\text{eff}}D\ , \quad (1)$$

where r_0 is the classical electron radius, c is the velocity of light, $n=n_L D$ is the number density of the gas, and D is the density in amagats. (The standard number density, which is often represented by the notation of n_0, is written n_L in this paper.) ${}^1Z_{\text{eff}}$ is the effective number of electrons per atom (molecule) in a singlet state relative to the positron of o-Ps. Also in N_2 gas, Eq. (1) holds good at room temperature. Griffith and Heyland[37] have reported that a linear relation is observed over the wide density range of 0–234 amagat, resulting in ${}^1Z_{\text{eff}}=0.260\pm0.005$. Our data measured at room temperature are in good agreement with their result.

Present low-temperature results are shown in Fig. 1 as a function of N_2 density. $\lambda_{o\text{-Ps}}$ increases linearly or almost linearly at lower densities and in the next region gradually deviates downward from the linear extrapolation of the low-density data. The overall behavior differs from that at room temperature mentioned above. The onset of the deviation is not clear-cut because of the very gradual nature of the transition. This feature resembles those observed in other gases such as CH_4,[38] C_2H_6,[22,23] CO_2,[24] and Ar,[12] and He (Ref. 39) and H_2 (Ref. 40) at 77 K.

${}^1Z_{\text{eff}}$ and a maximum density of the linear region D^* characterize the behavior of $\lambda_{o\text{-Ps}}$ in low densities. We have determined them by carrying out a weighted least-squares fit of Eq. (1) to the data together with a fixed value of $\lambda_{\text{vac}}=7.06\ \mu s^{-1}$. Our estimate of ${}^1Z_{\text{eff}}$ is 0.247 ± 0.002, 0.253 ± 0.005, 0.255 ± 0.003, and 0.253 ± 0.002 at 100, 120, 130, and 170 K,[41] respectively. There seems to be no apparent temperature dependence among them. The present values are only slightly lower than Griffith and Heyland's[37] result of 0.260 ± 0.005 at room temperature, and agree within the quoted standard deviations. Because of the small number of data points at low densities, ${}^1Z_{\text{eff}}$ and D^* are not estimated at 140 and 150 K. D^* is about 10, 11, 12, and 23 amagat at 100, 120, 130, and 170 K, respectively.[41] The fractional deviation of density, $(D-D_I)/D_I$, which serves as a measure of imperfection of real gases, is 0.08, 0.06, 0.05, and 0.06 at D^* at the same four temperatures. (D_I is a density of the ideal gas at the same temperature and pressure as the real gas.) The fractional deviations do not have a unique value, in contrast to the cases of CH_4 (Ref. 21) and C_2H_6 (Ref. 22) but the order of magnitude is in agreement with those in the above gases and CO_2 (Ref. 24).

Deviation of $\lambda_{o\text{-Ps}}$ from the linear dependence on density is observed at densities greater than D^*. The lower the temperature, the smaller the value of $\lambda_{o\text{-Ps}}$ at any given density. $\lambda_{o\text{-Ps}}$ deviates monotonically in the range up to densities near the liquid-gas phase boundary at 100 and 120 K, and in the entire range of the present measurement at 150 and 170 K. At 130 K, it is observed that there exists an inflection point at around 200 amagat and above this region $\lambda_{o\text{-Ps}}$ no longer decreases. A similar trend is also seen at 140 K, although the data are limited in the higher densities. The nonlinear density dependence of $\lambda_{o\text{-Ps}}$ is further clarified by looking at a behavior of the empirical parameter ${}^1Z_{\text{eff}}$ calculated from Eq. (1). Ratios of ${}^1Z_{\text{eff}}$ to ${}^1\tilde{Z}_{\text{eff}}=0.260$, as a reference, are plotted as a function of density in Fig. 2. The higher the temperature, the smaller the departure of the ratio from unity. At 130 and 140 K, the minimum exists at about 300 amagat and the ratio increases again after that. It is interesting to notice that this feature is analogous to the compressibility factor Z of N_2, which is equal to a ratio D_I/D. At room temperature, the ratio ${}^1Z_{\text{eff}}/{}^1\tilde{Z}_{\text{eff}}$ is constant at unity up to $\sim$200 amagat, resulting from the linear dependence of $\lambda_{o\text{-Ps}}$ on density.[37] This also agrees with the value of Z of N_2 being nearly equal to unity over a wide density range at room temperature. A similar analogy appears to hold well for other gases. For Ar, for example, at 160 K, the ratio increases again after the initial decrease and seems to reach unity at the density of $\sim$690 amagat,[12] and this feature resembles the variation of Z in that it becomes unity again at $\sim$630 amagat after the minimum at around 400 amagat.[32] Also, for C_2H_6, a similar feature can be seen,[23] but the fitting to the variation of Z (Ref. 42) is less than those in the cases of N_2 and Ar. It should be also noticed that the behavior of the ratio in low-temperature He shows a different feature from those in the above gases. The abrupt and large decrease of the ratio with increasing density at 6 and 10 K (Ref. 8) is in contrast to the smooth decrease of Z at the corresponding temperatures.[43] The ratios become considerably smaller than unity even at the higher temperatures, where $Z>1$.

In connection with the analogy between the ratio and Z, it is interesting to note that $\lambda_{o\text{-Ps}}$ increases almost linearly with pressure over wide ranges. It is not surprising that such a linear relation is observed in a sufficiently low-pressure range because at low pressures the real gas density does not differ greatly from the ideal gas density which is proportional to the pressure. This relation, however, extends to comparatively high-density data points above D^*.[44] Figure 3 shows plots of $\lambda_{o\text{-Ps}}$ against

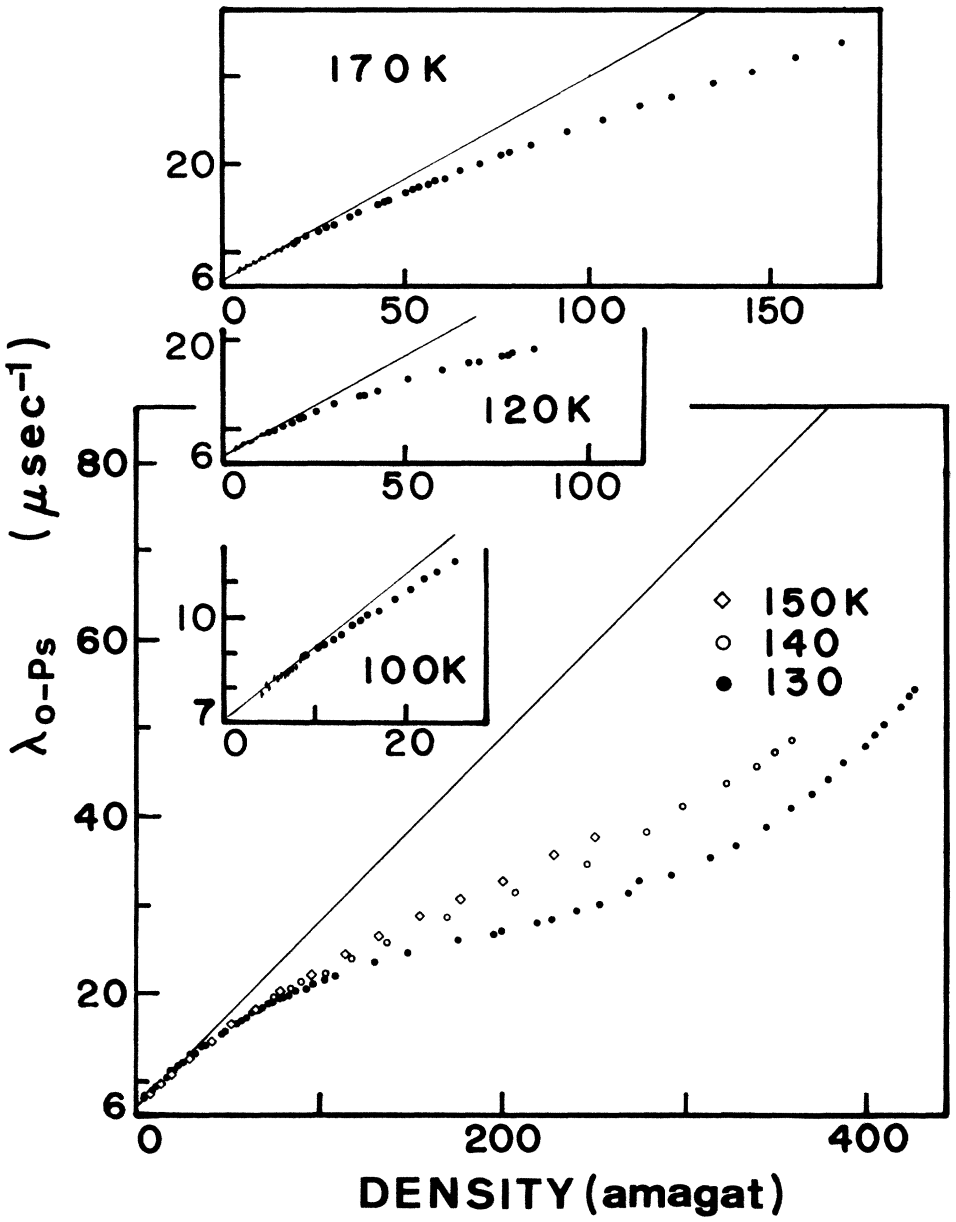

FIG. 1. $\lambda_{o\text{-Ps}}$ vs N_2 density at various temperatures. The statistical standard deviations fall within the size of the points unless otherwise shown. The solid lines represent Eq. (1) with the values of $\lambda_{vac}=7.06\ \mu s^{-1}$ and ${}^1Z_{eff}=0.260$.

P/T, where P and T are the pressure and temperatures of the gas, respectively. At room temperature the value of Z is almost equal to unity over a wide density range. From the observation of the linear dependence of $\lambda_{o\text{-Ps}}$ on density and the good approximation of the real density by the ideal gas density, which is proportional to P, it is guessed that the linear relation between $\lambda_{o\text{-Ps}}$ and the pressure holds well also at room temperature in N_2. The value of ${}^1Z_{eff}=0.260$ can be translated to the value of the slope 57.1 μs^{-1} atm^{-1} K of the $\lambda_{o\text{-Ps}}$ versus the P/T plot. The linear relation between $\lambda_{o\text{-Ps}}$ and P/T seems to hold well in low and intermediate density ranges over a fairly wide temperature range. A similar result for Xe has been reported by Tseng *et al.*[45]

III. APPLICATION OF CURRENT MODELS AND DISCUSSION

We discuss in this section the behavior of *o*-Ps in low-temperature N_2 in terms of current models where applicable.

A. Density-functional method

The density-functional method is a sophisticated approach that gets around the defect of the square-well model. For a system of an *o*-Ps plus classical fluid at temperature T and chemical potential μ, the grand free energy as a functional is written as

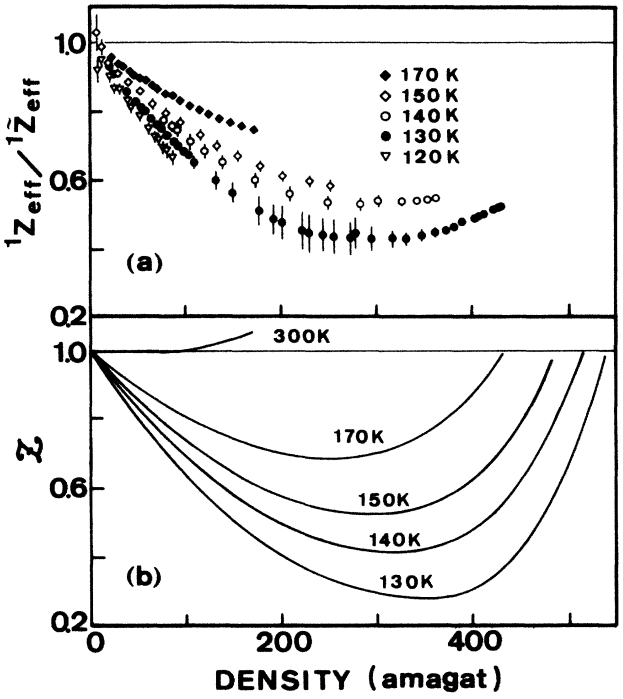

FIG. 2. (a) Ratios of $^1Z_{eff}/^1\tilde{Z}_{eff}$ vs N_2 density at various temperatures, where $^1\tilde{Z}_{eff}=0.260$. Some of the low-density data points are omitted for clarity. The line of the ratio equal to 1.0 corresponds to the linear dependence of $\lambda_{o\text{-}Ps}$ on density at room temperature (Ref. 37). (b) Density dependence of the compressibility factor Z. The curves are calculated by using the equation of state for N_2 (Ref. 31).

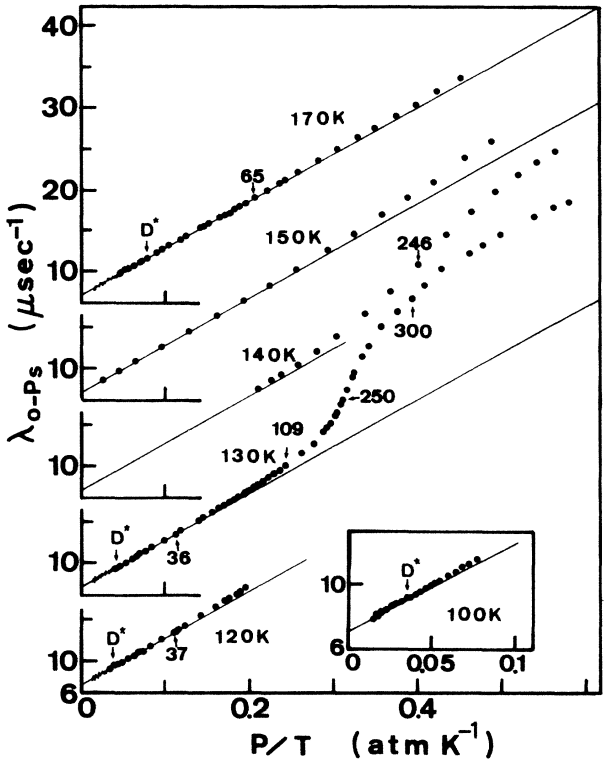

FIG. 3. $\lambda_{o\text{-}Ps}$ vs P/T at various temperatures. Letters by the symbols indicate the density and D^* are the critical densities of the linear dependence of $\lambda_{o\text{-}Ps}$ on density. The slope of the solid lines is 57.1. See text for further details.

$$\Omega[n]=F[n]-\mu\int d\mathbf{r}\, n(\mathbf{r})+\int d\mathbf{r}\, V(\mathbf{r})\,|\psi(\mathbf{r})|^2 + \frac{\hbar^2}{2m_p}\int d\mathbf{r}\,|\nabla\psi(\mathbf{r})|^2 , \quad (2)$$

where $F[n]$ is the free energy of the inhomogeneous fluid, $n(\mathbf{r})$ is the fluid molecule number density, $\psi(\mathbf{r})$ is the o-Ps wave function, m_p is the Ps mass, and $V(\mathbf{r})$ is the mean potential, produced by the fluid molecules, in which o-Ps moves. The minimization of the functional with respect to variations of $n(\mathbf{r})$ and $\psi(\mathbf{r})$ yields two Euler equations. These equations are usually solved together self-consistently, and then the density profile and the o-Ps wave function are obtained. As one is mainly interested in the free-energy difference between the localized state and the extended state in a homogeneous fluid, the change in the grand free energy, $\Delta\Omega[n]\equiv\Omega[n]-\Omega[n_0]$, is often used, for convenience, where n_0 is the density of the homogeneous fluid far from the bubble. The bubble state is possible when $\Delta\Omega$ has a minimum with an inhomogeneous density profile. The bubble is stable with $\Delta\Omega<0$ and metastable with $\Delta\Omega>0$.

The potential $V(\mathbf{r})$ is approximated by $E_\infty(n(\mathbf{r}))$ when the density changes slowly in the scale of the range of o-Ps–molecule interaction, where $E_\infty(n)$ is the energy whereby a homogeneous fluid with density n shifts the o-Ps energy. In the present calculation, $E_\infty(n)$ is approximated by the optical potential

$$E_\infty(n)=\frac{2\pi\hbar^2 a_s n}{m_p} , \quad (3)$$

where the scattering length a_s plays the role of an adjustable parameter to fit the calculation to the experimental pickoff rates. For $F[n]$, the local-free-energy approximation

$$F[n]=\int d\mathbf{r}\, f(n(\mathbf{r}))$$

is used, where $f(n)$ is the Helmholtz free-energy density of a homogeneous fluid, which is calculated by using the semiempirical equation of state.[31]

In the numerical procedure, rather than solving the Euler equations directly, we employ a procedure similar to that of Ebner and Punyanitya.[18] Assuming an appropriate form of $n(\mathbf{r})$, the Schrödinger equation of o-Ps is solved first:

$$-\frac{\hbar^2}{2m_p}\nabla^2\psi(\mathbf{r})+\frac{2\pi\hbar^2 a_s}{m_p}[n(\mathbf{r})-n_0]\psi(\mathbf{r})=\varepsilon\psi(\mathbf{r}) , \quad (4)$$

where ε is the lowest-energy eigenvalue. As the lowest state is considered, ψ depends on r alone, and Eq. (4) is reduced to a radial equation. The density n is also a function of r alone, and a simple form[18] $n(r)=n_0-\alpha/e^{(r-\beta)/\gamma+1}$ is assumed in the present calculation, where α, β, and γ are adjustable parameters.[18] Using $n(r)$ with a

certain set of three parameters, the radial equation is solved numerically. Then, $\Delta\Omega \equiv \Omega[n] - \Omega[n_0]$ is calculated, using the assumed $n(r)$ and the resulting ε. Adjusting the parameters on a suitable size grid, a reliable local minimum of $\Delta\Omega$ at homogeneous density n_0 is obtained. Finally, the pickoff annihilation rate λ_p is evaluated. Avoiding the difficulty of the treatment of excited states of the bubbles, we calculate λ_p using a two-state approximation

$$\lambda_p = \frac{\lambda_\infty(n_0) e^{\Delta\Omega/kT} + \lambda_b}{e^{\Delta\Omega/kT} + 1} , \tag{5}$$

where $\lambda_\infty(n_0)$ is the pickoff rate of o-Ps in the extended state in the homogeneous fluid with density n_0, and λ_b is the pickoff rate for the bubble state. $\lambda_\infty(n)$ is estimated assuming the linear relation $\lambda_\infty(n) = 4\pi r_0^2 c n\, {}^1Z_{\text{eff}}$ with ${}^1Z_{\text{eff}} = 0.260$. λ_b is calculated from the equation

$$\lambda_b = \int d\mathbf{r}\, \lambda_\infty(n(\mathbf{r})) \, |\psi(\mathbf{r})|^2 . \tag{6}$$

Results of λ_p for several different values of a_s are shown in Fig. 4. For a trial value $a_s = 0.8$ Å, $\Delta\Omega$ is negative in the density range $190 \lesssim n_0 \lesssim 450$ amagat, which is the stable bubble region. The calculated values are in agreement with the experimental data within $\pm 20\%$ in the range $280 \lesssim n_0 \lesssim 430$ amagat. At higher densities, the calculated value rapidly increases almost linearly toward the extrapolated line of $\lambda_\infty(n)$, which has not yet been explored experimentally. For $a_s = 0.7$ Å, the calculated values are, as a whole, larger than the experimental data, reflecting small and shallow bubbles due to the weak repulsion. In both cases, the calculated values of λ_p are considerably larger than the experimental values at densities less than about 250 amagat and display a different trend from the experimental behavior which shows a monotonic decrease. An especially obvious discrepancy exists at the onset region of deviation. If the value of a_s is increased, the onset shifts to the lower densities. However, results with the larger value of $a_s = 1.0$ Å, for example, show poorer agreement with the experiment at higher densities. For the calculation with $a_s = 0.8$ Å, $\Delta\Omega$ is at most $-2.8kT$ and so the bubble is only weakly stable. For $a_s = 1.0$ Å the bubble is more stable with at most $\Delta\Omega \simeq -6kT$. This situation is comparable with the case of Ar,[12] but contrasts with that of He in which the o-Ps bubble is quite stable with $\Delta\Omega$ of order $100kT$.[12] Figure 5 shows some density profiles of the bubble. The corner of the bubble is round and some residual gas molecules exist in it. The calculation of λ_p at 140 K has also been carried out with $a_s = 0.8$ Å, yielding considerably larger values than the experiment. The bubble is metastable in all the range calculated and its profile is shallow and smooth. For higher temperatures, the local minimum of $\Delta\Omega$ is not found in the present calculation with the chosen form of $n(r)$, its parameters, and the sizes of grids used.

The optical potential used in the calculation is the simplest approximation to $E_\infty(n)$. In dense gases, however, it is probable that this potential gives an underestimate of the real $E_\infty(n)$. The Wigner-Seitz method[46] is the alternative way often used which may provide a good approximation to $E_\infty(n)$ for higher densities. This method indeed provided a result which is in good agreement with the barrier height measured by an experiment of electron injection from He gas into liquid He.[47] In Fig. 6, values of $E_\infty(n)$ for o-Ps in N_2 gas are shown for various values of a_s as a parameter. $E_\infty(n)$ by the Wigner-Seitz method are considerably larger than the optical potential with the same a_s. Density-functional calculations using the Wigner-Seitz $E_\infty(n)$ with $a_s = 0.8$ Å will give values of λ_p less than those with $a_s = 1.0$ Å in Fig. 4. The Wigner-Seitz $E_\infty(n)$ with a_s around 0.55 Å are different only within about 10% from the optical potential with $a_s = 0.8$ Å in the stable bubble region. Therefore, the calculation using $E_\infty(n)$ by the Wigner-Seitz method with 0.55 Å will give similar results to the calculation with 0.8 Å in Fig. 4.

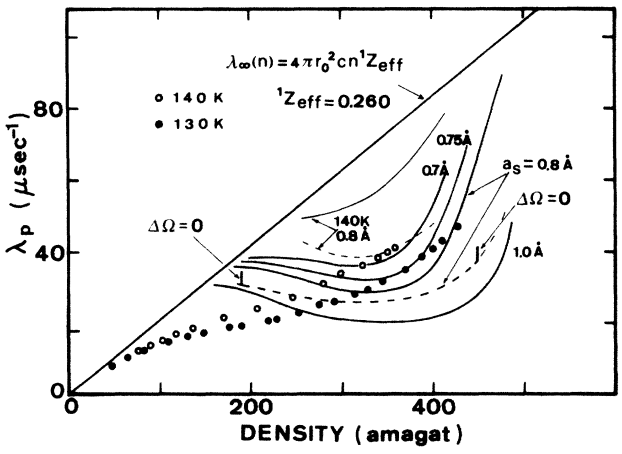

FIG. 4. Theoretical and experimental pickoff annihilation rates as a function of N_2 density at 130 and 140 K. At 130 K, the theoretical curves are calculated for four different scattering lengths. The solid curves represent the total pickoff rates and the dashed curves the pickoff rates for the o-Ps in the bubble states.

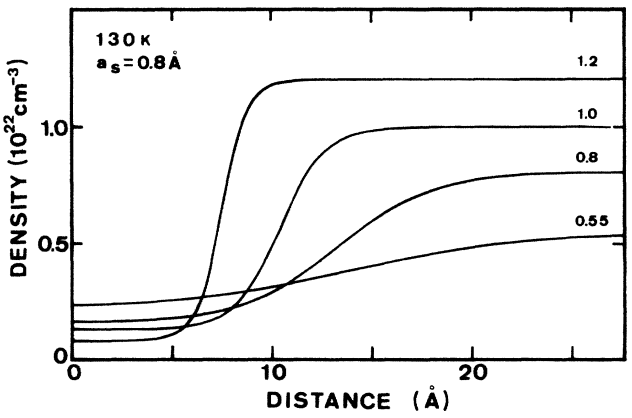

FIG. 5. Density profiles around o-Ps at different densities at 130 K for a scattering length of 0.8 Å. Letters indicate the density.

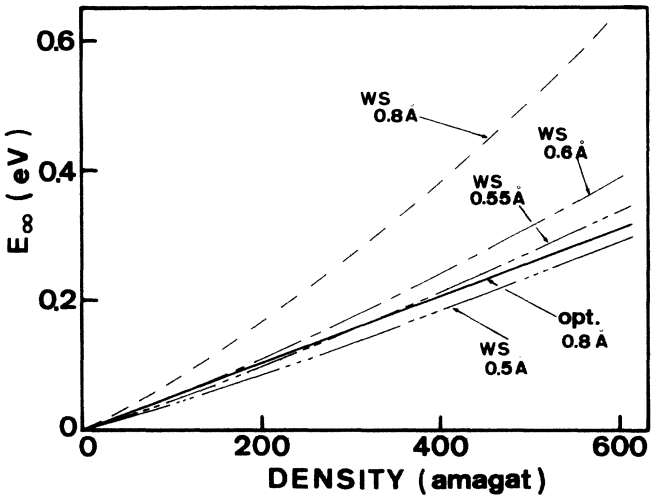

FIG. 6. E_∞ vs N_2 density. The solid line is calculated by the optical potential model with a scattering length of 0.8 Å. The others are calculated by the Wigner-Seitz model with four different scattering lengths.

In the calculation shown in Fig. 4, the linear relation has been assumed for the density dependence of $\lambda_\infty(n)$. This relation, in fact, has been experimentally observed over a wide density range at room temperature in gases such as He,[39] Ar, H_2, CO, and also N_2.[37] Validity of the use of this relation, therefore, may be supported in these density ranges. It is unknown, however, whether the linear relation also holds well even at much higher densities than these ranges. Ferrell obtained a correction to the linear relation of $\lambda_\infty(n)$ in high-density He within the Wigner-Seitz model.[1,7] This correction arises from the normalization of the o-Ps wave function in the region which is allowed for o-Ps avoiding a volume occupied by the He atom due to the repulsive interaction. This method yielded a nonlinear density dependence, but values of $\lambda_\infty(n)$ were considerably larger than the experimental values which were found to be linearly dependent on density. In the N_2 case, this also provides results contradictory to the experimental observation, that is, $\lambda_\infty(n)$ is 1.6-fold larger than the experiment at 100 amagat and 1.8-fold larger than that at 200 amagat.

For $E_\infty(n)$ and $\lambda_\infty(n)$ in He, Nieminen *et al.*[9] calculated corrections to the Wigner-Seitz model by using a pseudopotential method, which was introduced by Stott and co-investigators[48] to calculate a positron distribution in solids. This calculation provided values of $\lambda_\infty(n)$ which reasonably agree with the existing experimental data, but gave values considerably smaller than the Wigner-Seitz calculations. Tuomisaari *et al.*[12] also applied this method to the Ar case. They used a pair potential including an attractive tail, that is, the Buckingham type or the Lennard-Jones type, for the Ps-Ar potential. The calculation yielded too many stable bubbles and gave annihilation rates in poorer agreement with the experimental data compared with those calculated by using the Wigner-Seitz energy model. Such an approach may be applicable for the N_2 case, but it is considerably troublesome to carry out the procedure using an appropriate Ps-N_2 pair potential.

As described above, it is indicated by the density-functional calculation that the o-Ps bubble exists at low temperature near T_c and the reduction of the o-Ps annihilation rate is attributed to the bubble formation, at least in the higher-density region at 130 K. The o-Ps–N_2 scattering length is estimated to be about 0.8 Å with the calculation which provides better fits to the experimental data with the optical potential. This value may correspond to around 0.55 Å for $E_\infty(n)$ by the Wigner-Seitz method. At lower densities at 130 K, the present calculation fails to explain the gradual downward deviation. Also, for higher temperatures, this calculation does not provide good results.

B. Density-fluctuation model

The density-fluctuation model is an approach which relates the deviation of the o-Ps annihilation rate from the linear dependence to using the density fluctuations in gases, using classical thermodynamics. It is known that this model provides good fits to the experimental data in several gases for density ranges where the deviations are relatively small in magnitude.

McNutt and Sharma have measured $\lambda_{o\text{-Ps}}$ in CH_4 and observed that there exists a linear relation between $(D-D_I)/D_I$, the fractional density deviation, and $\Delta\lambda$, the deviation of the measured $\lambda_{o\text{-Ps}}$ from the value linearly extrapolated from low-density data.[21] From this correlation, it is suggested that the downward deviation in CH_4 is not due to the bubble formation, but rather due to the density fluctuations existing in an imperfect gas. Namely, o-Ps may preferentially migrate into regions with density lower than the average density, resulting in the reduction of the annihilation rate. By correlating $\Delta\lambda$ directly with the density-fluctuation distribution in gas, they have proposed the "density-fluctuation model."

In this model, the distribution of a relative density fluctuation δ from the equilibrium density in a small cell of volume V_0 with o-Ps samples is considered. Using a probability distribution of the fluctuation δ, and assuming that o-Ps atoms sample regions in which the time-averaged density is lower than the equilibrium, McNutt and Sharma found the relation

$$\Delta\lambda = 4\pi r_0^2 c n_L \, {}^1Z_{\text{eff}} D (kTK_0/2\pi V_0)^{1/2} , \tag{7}$$

where K_0 is the isothermal compressibility of the gas. In this model, V_0 is assumed to be independent of gas density, and one can derive the volume from the slope of this linear relation found in the data, if any.

In Fig. 7, $\Delta\lambda$ is plotted as a function of $D(kTK_0)^{1/2}$. At 130 K, $\Delta\lambda$ is around zero at the lowest-density region, and after a somewhat concave region the linear relation is observed in the range corresponding to the data with densities up to about 110 amagat. The volume V_0 derived from the slope corresponds to a sphere of a radius of approximately 5.6 Å. The prediction of this model obviously breaks down at densities higher than about 250

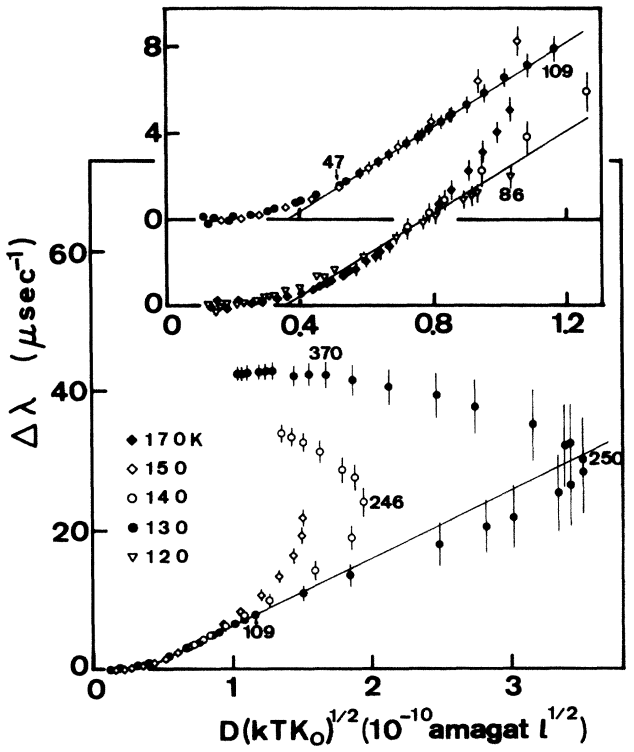

FIG. 7. Deviations $\Delta\lambda$ vs $D(kTK_0)^{1/2}$ at various temperatures. The inset shows the data in the lower-density regions. The statistical standard deviations fall within the size of the points unless otherwise shown. The solid lines represent a weighted least-squares fit to the data for the densities 47–109 amagat at 130 K. Letters by the symbols indicate the density. Some of low-density data are omitted for clarity.

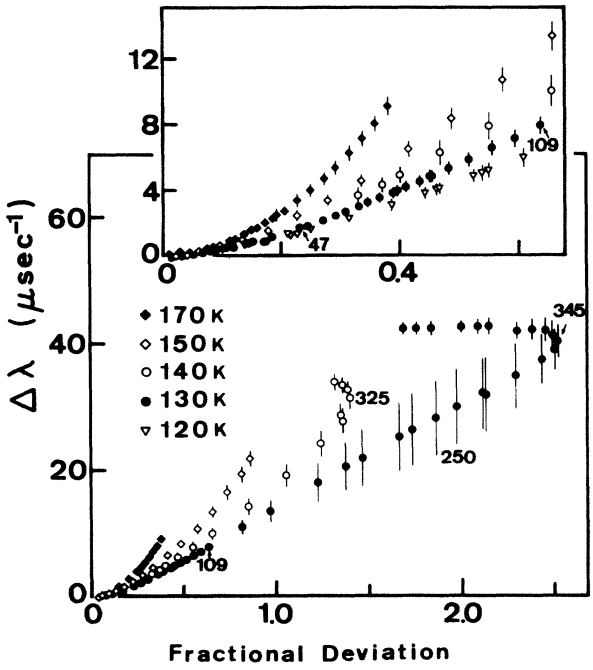

FIG. 8. Deviations $\Delta\lambda$ vs fractional deviations $(D-D_I)/D_I$ at various temperatures. Letters by the symbols indicate the density. The inset shows the low-density data.

amagat, which is the region where the behavior of $\lambda_{o\text{-Ps}}$ has been reasonably explained by the bubble model. At 120 K, the plot is in good agreement with that at 130 K. The plot for 140 K shows a similar trend to 130 K. For 150 and 170 K, the plot shows a concave shape as a whole, although partially overlaps to the linear region of 130 K.

As mentioned above, this model provides the sampling volume which corresponds to a sphere with a diameter of an order of 10 Å or a cubic cell with a side of the same order. This sampling length is far less than the *o*-Ps thermal wavelength of ~ 80 Å. The size of the sampling volume is smaller than that of the typical bubble in Fig. 5 estimated by the density-functional calculation. In the linear region of this model, about 50–100 amagat, this volume contains only 1–2 molecules as an average density. This situation on the sampling volume is also true for Ar at 160 K.[12] The density-fluctuation model provides at least a qualitative explanation of the not very large deviations in N_2, as in the cases of other gases, but seems to have a difficulty on the size of the sampling volume which it derives from experimental data.

In connection with the prediction of this model, it is worth examining correlations between $\Delta\lambda$ and some quantities which may serve as a measure of density fluctuations in N_2 gas. In Fig. 8, the values of $\Delta\lambda$ are plotted as a function of the fractional deviation. $\Delta\lambda$ depends linearly on the fractional deviation in certain ranges, although at higher temperatures it shows a somewhat concave shape of dependence as a whole. This linear relation corresponds to similar observations by McNutt and Sharma in their study of CH_4 (Ref. 21) and C_2H_6 (Ref. 22). It may be also noted, on the other hand, that the present plots show a distinct difference from those of C_2H_6 in the region where the linear relation breaks down. The plot turns upward from the linear relation in the present case, and downward in C_2H_6.[23] The upward turning has been observed also in Ar.[12]

Figure 9 shows plots of $\Delta\lambda$ against the density difference D-D_I. Linear relations are found over wide ranges at all temperatures.[49] This linear relation is similar to the observation in CO_2 at room temperature by Wright *et al.*,[24] and is related to the dependence of $\lambda_{o\text{-Ps}}$ on the pressure of the gas. These correlations suggest the significance of the role of density fluctuations to the *o*-Ps behavior in the gases, but have not been directly treated by the theory of the *o*-Ps annihilation behavior in gas. A full explanation of these observations remains open.

C. Application of the Eggarter-Cohen approach to the *o*-Ps problem

The role of density fluctuations in the *o*-Ps behavior may be treated from a quantum-mechanical point of view. In this treatment, one imagines that the density fluctuation in gases gives rise to a fluctuation of the po-

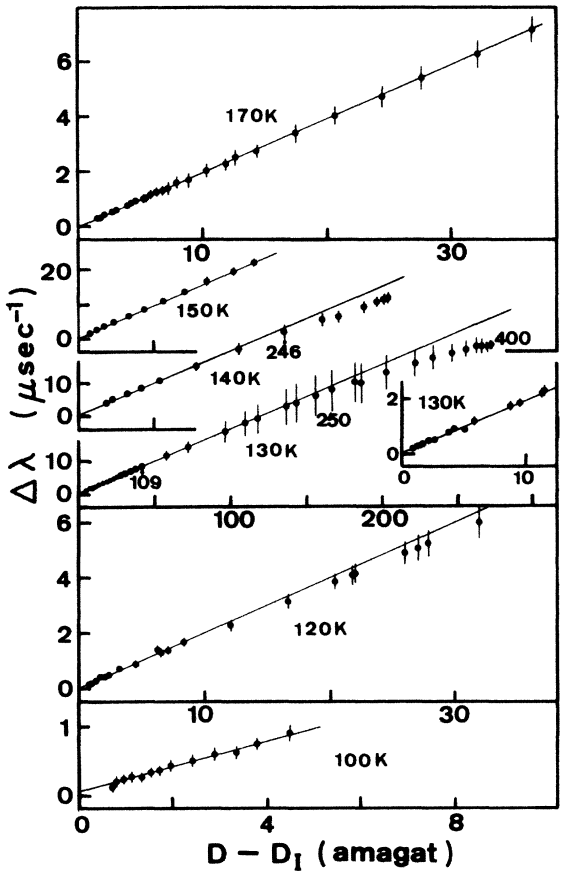

FIG. 9. Deviations $\Delta\lambda$ vs density differences $D-D_I$ at various temperatures. The data for the densities $D \lesssim D^*$ are omitted. The solid lines represent weighted least-squares fits to the data satisfying both inequalities $D > D^*$ and $D-D_I < 10$ amagat (Ref. 49). At 130 K, the maximum value of $D-D_I$ corresponds to $D \simeq 400$. The inset shows the low-density data at 130 K.

tential in which o-Ps moves. The states available to a light particle in disordered materials have states localized by the potential fluctuations in the Anderson sense. From the repulsive o-Ps–gas interaction, it is considered that the o-Ps in such states is sampling a lower density than the average. There have been a few studies to understand the reduction of the o-Ps annihilation rate (and the rapid drop of the electron mobility which is closely related to the o-Ps case) within this context.

Hernandez and his co-workers have applied a variational method to these problems.[28,29] They have examined the influence of the physical parameters such as the scattering lengths, the packing fraction, the relative atomic sizes, and the density to the light-particle state and its localization. It has been shown that the observed trends in the o-Ps annihilation rates in gases (and also in the electron mobility in low-temperature He) conform to the trends predicted by their calculations. However, these calculations have not yet produced the quantitative predictions for comparison with the experimental data on the o-Ps annihilation rate and the excess electron mobility, because the theoretical basis is a variational method.

Prior to the above calculations, Eggarter and Cohen (EC) have developed a semiclassical approach treating the effect of density fluctuations to the excess-electron mobility in low-temperature gaseous He.[26,27] Their model is simple in the procedures of calculation of the density of states, and of the estimation of the fraction of localized states. The method has succeeded in explaining the rapid decrease of the electron mobility by introducing energy-dependent mobilities of the electron both in extended and localized states. The semiclassical counting of the density of states and the percolation theory for the localization employed in this model may be applicable to the o-Ps problem.

In the EC model, a total system is divided into cubic cells with a volume L^3, where

$$L \equiv c_0 2\pi\hbar(3/2mE)^{1/2}$$

is an order of a de Broglie wavelength of an electron with an energy E, m is the particle mass, and c_0 is an adjusting parameter of an order of 1. The assumption that the density in each cell is constant gives rise to an effective potential for an electron, $V(n)$, the Wigner-Seitz potential, where $n = N/L^3$; N is a number of atoms in the cell. The number of atoms in the finite volume L^3 fluctuates and its distribution is considered to be a Gaussian about $\bar{N} = \bar{n}L^3$ with the standard deviation σ_N, where $\bar{n}$ is the average density and σ_N is calculated taking into account the non-ideal-gas dependence of pressure on density. This gives rise to the fluctuating potential $V(n)$ with a Gaussian distribution about $\bar{V}$. Adding a cell density of states over cells in the total system, a density of states $n(E)$ is obtained. The fraction of extended electron states at a given energy is provided by the classical percolation theory.[50] The percolation theory provides a critical energy, E_c. At energies less than E_c, the percolation probability is strictly zero and increases monotonically to unity above E_c.

According to this model, the change of electron mobility in low-temperature He as a function of the average gas density is qualitatively interpreted as the following: The function $n(E)e^{-E/kT}$ has a maximum at $E_{\max}$ and it is sharply peaked. For low densities this peak occurs over $\bar{V}$ and the dominant fraction of electron is in extended states. As the average density increases, $E_{\max}$ shifts from a higher to a lower side than E_c. This means that the fraction of electrons in localized states increases. Therefore, the mobility drastically decreases several orders of magnitude in this density range because of the small mobilities of electrons in localized states. For high densities, finally, $E_{\max} \ll E_c$ and practically all electrons are in localized states. The theoretical mobility is calculated by using this function, introducing energy-dependent mobilities for both in the extended and localized states.

The discussion on the distribution of states given by this model may also be applicable to the o-Ps case. The result derived, however, is significantly affected by selection of the value of the parameter c_0, which was determined, in the electron case, by adjusting calculated mobilities to experimental data. Therefore, we attempt

first to apply this model to the problem of o-Ps in low-temperature He gas because this case may be quite analogous to that treated by the original EC model. For the o-Ps–He scattering length and the potential $V(n)$, we owe to the bubble model analysis,[8,9] concretely, $a_s = 0.79$ Å and values of the optical potential. The non-ideal-gas dependence of pressure with density is taken into account.[43]

The function $n(E)e^{-E/kT}$ for Ps in He shows a similar trend to the electron case. Isothermally the fraction of o-Ps in localized states increases with increasing density. The higher the temperature, the broader the function in energy. Figure 10 shows the variation of the function for a particular case of $c_0 = 1.0$ at 6 K. (In the original EC model, the best fit to experimental data at about 4–20 K was obtained with $c_0 = 1.05$–1.4,[51] using a smaller value at a higher temperature.) The peak of $n(E)e^{-E/kT}$ positioned at E_{max} shifts from a higher to a lower energy than E_c while increasing density isothermally in the density region between ρ_1 and ρ_2, where ρ_1 is the experimentally obtained density deviation onset[8] and ρ_2 the critical density of the stable bubbles theoretically predicted by the density-functional method.[9] A small variation of c_0 does not change the qualitative feature, but small or large values of c_0 (for example, $c_0 = 0.6$ or 2.0) yield distributions in disagreement with experimentally or theoretically accepted knowledge. This strongly suggests that this model reasonably represents states of o-Ps in low-temperature He, with appropriate c_0. We further proceed to connect this result directly with the calculation of the pickoff rate λ_p. We first assume that o-Ps in the extended state annihilates to sample the average density $\bar{n}$ and therefore, the pickoff rate of this o-Ps, λ_{ext}, is $4\pi r_0^2 c\bar{n}\,{}^1Z_{eff}$. On the other hand, since a localized o-Ps with an energy E exists in a cell with density lower than $n_{max}(E)$, which is the maximum density satisfying an inequality $V(n) > E$, its o-Ps samples the density $n_{max}(E)$ at most. We assume that the density sampled by the localized o-Ps with energy E is approximated by the average value $n_{av}(E)$. $n_{av}(E)$ is further approximated by $c_0' n_{max}(E)$, c_0' being another adjusting parameter. Ultimately, the pickoff rate of such an o-Ps, λ_{loc}, is assumed to be

$$\lambda_{loc}(E) = 4\pi r_0^2 c\,{}^1Z_{eff} c_0' n_{max}(E) .$$

The total pickoff rate of o-Ps with energy E, $\lambda_p(E)$, is written as

$$\lambda_p(E) = 4\pi r_0^2 c\,{}^1Z_{eff}\{[1-P(E)]c_0' n_{max}(E) + P(E)\bar{n}\} , \tag{8}$$

where $P(E)$ is the same percolation probability as in the original EC model. Finally, λ_p is calculated from the equation

$$\lambda_p = \frac{\int \lambda_p(E) n(E) e^{-E/kT} dE}{\int n(E) e^{-E/kT} dE} . \tag{9}$$

By using Eq. (9), a ratio of calculated λ_p to extrapolation of the linear region is obtained.[39] Good agreement with the experiment has been obtained at temperatures of 6–40 K, as shown in Fig. 11(a). Small variations of c_0 and c_0' do not yield very different results, but they generally give poorer agreement. At 30 and 40 K, similar results are given by using $c_0' = 0.7$ and a fairly small value of $c_0 = 0.6$, but this usage fails at lower temperatures. It should be noted that this model, although a rough approximation, gives good results over a wide temperature range by using a unique value of c_0 and values of c_0 analogous to the original EC model for an electron,[27] and, furthermore, the density range treated is the range at which the density-functional calculation has shown a discrepancy with the experiment.[9] The result described above supports the assertion that the treatment of o-Ps states in low-temperature He by the present model is reasonable and that the present estimation of λ_p is not invalid.

When the present model was applied to the N_2 problem, however, no good result unfortunately was obtained. Reflecting a smooth change of the factor of $e^{-E/kT}$

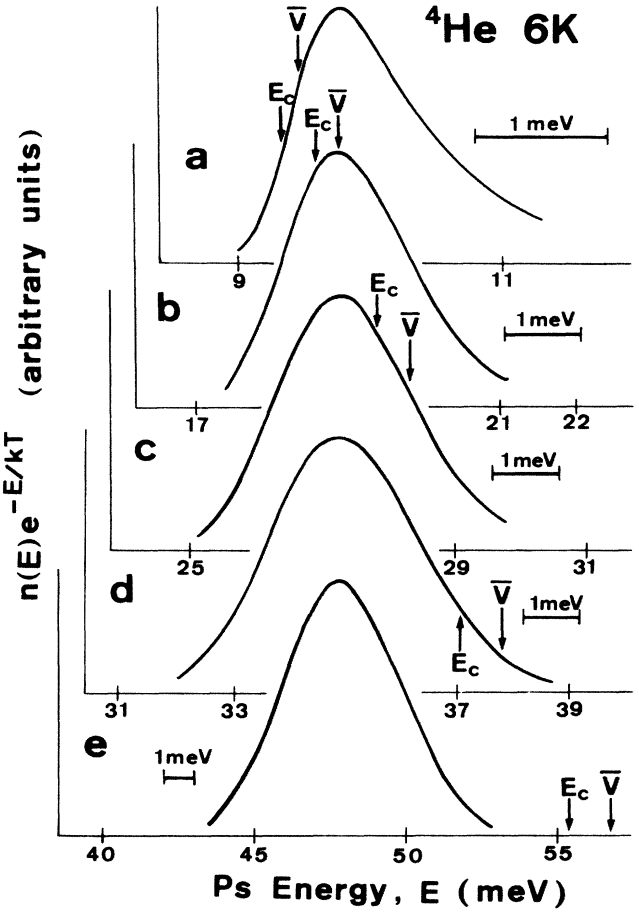

FIG. 10. A function $n(E)e^{-E/kT}$ for $c_0 = 1.0$ in He at 6 K at various densities: a, 0.05; b, 0.1; c, 0.15; d, 0.2; and e, 0.3 ($\times 10^{22}$ cm^{-3}). $\bar{V}$ and E_c are the average potential and the critical energy, respectively. ρ_1 is about 0.09×10^{22} cm^{-3} (Ref. 8) and ρ_2 is about 0.23×10^{22} cm^{-3} (Ref. 9).

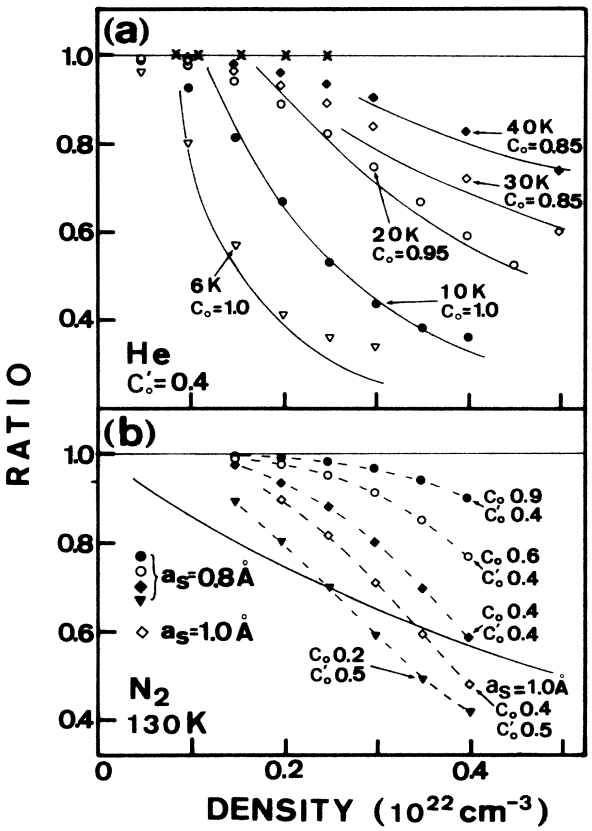

FIG. 11. (a) Ratios of λ_p calculated by Eq. (9) to the linear extrapolation of the data for He measured by Fox *et al.* (Ref. 39). The crosses indicate the transition densities for *o*-Ps from free to bubble state measured by Rytsölä *et al.* (Ref. 8). The solid curves represent the density dependence of the ratios of the experimental λ_p (Ref. 8). (b) Calculated ratios for N_2 at 130 K for scattering lengths of 0.8 and 1.0 Å. The dashed curves are drawn to guide the eye. The solid curve represents the density dependence of the present experimental ratios.

against E due to the high temperatures, the function of $n(E)e^{-E/kT}$ has a long tail extending over a higher-energy side and is not very sharply peaked, in general, at the region except for at high densities. Therefore, the contribution of the *o*-Ps in localized states is considerably small in comparison to the total pickoff annihilation rate calculated by Eq. (9). With use of the optical potential and the scattering length $a_s = 0.8$ Å, the values of the calculated ratio with c_0 near 1 show a weak density dependence, as shown in Fig. 11(b). The value of the ratio becomes comparable with the experimental data and the value of the ratio varies rapidly as the value of c_0 is considerably decreased from 1. However, the corresponding sampling length which is somewhat smaller than the de Broglie wavelength is unclear in the physical meaning and inconsistent with the original EC model.[27] Provided that the larger value of a_s is used, one can adopt somewhat large values of c_0 for the calculation, but this change does not improve the discrepancy. Thus, the present model does not provide a good fit to the experimental data of N_2. The difference of the magnitudes of the thermal energies might relate to a different quality of fits to the experimental data between the low-temperature He and the present N_2.

Our model has a defect in that the calculated pickoff rate does not always agree with the value calculated for the *o*-Ps trapped in the stable bubble by the bubble model in the higher-density region. The pickoff rate of *o*-Ps is calculated by using the wave function of *o*-Ps and the density distribution which *o*-Ps samples. However, it is very difficult to characterize the wave function of *o*-Ps weakly localizing in fluctuations and the density profile of its region. In the original EC model, the authors have characterized a size of a pseudobubble (equal to a trapped electron plus a low-density region) by translating the difference of a number of atoms in a cell from the average number to a volume of an empty sphere. This seems to be inappropriate for the *o*-Ps case since the calculation of the annihilation rate may require a more realistic feature of the object than the mobility. At energies $|E - E_c| \simeq kT$, even the characterization of the pseudobubble used in the EC model is not justified. Fortunately (or unfortunately in the sense that the information at these interesting energies is obscured), this model provides a good fit to the experimental data in spite of this serious problem because it is masked by the fairly high mobilities of extended electrons. In the *o*-Ps case, the treatment of this energy range may be important for specific predictions of the pickoff rate comparable with the experimental data.

IV. CONCLUSION

Deviation of the *o*-Ps annihilation rate from the linear dependence on density has been observed in low-temperature N_2. Linear relations have been found between the deviation and the quantities such as the fractional deviation and the density difference for intermediate magnitudes of the deviation. The ratio of the measured pickoff rate to the linear extrapolation has shown a density dependence similar to that of the compressibility factor of N_2 gas. In connection with the above observations, a linear relation has been found between the pickoff rate and P/T over wide pressure and temperature ranges.

The density-functional calculation using the optical potential for the *o*-Ps–gas interaction energy has indicated that *o*-Ps–induced bubbles exist in the higher-density region, at least at 130 K, and that the reduction of the *o*-Ps annihilation rate in this region is mainly due to this phenomenon. An *o*-Ps–N_2 scattering length of about 0.8 Å is obtained by this calculation.

The relatively small deviation at relatively low densities can be explained, at least qualitatively, by the density-fluctuation model. In order to obtain more insight into the role of density fluctuations in *o*-Ps behavior, the new approach, which owes much to the model by Eggarter and Cohen, has been attempted to solve the *o*-Ps annihilation problems. Our approach has provided reasonable results for low-temperature He, but has given no good results for N_2.

It is probably safe to say that the behavior of the *o*-Ps

annihilation rate in low-temperature N_2 can be understood by connecting the density-fluctuation effect in lower densities with the formation of *o*-Ps bubbles in higher densities. Our understanding is, however, unsatisfactory from a quantitative point of view. A more sophisticated theory is hoped for which can provide a sufficient explanation throughout, from the region where existing density fluctuations play a dominant role to that where *o*-Ps actively influences the environment around itself.

ACKNOWLEDGMENTS

The authors wish to thank the staffs of the Laboratory of Nuclear Radiation of the Institute for Chemical Research and the Radioisotope Research Center, Kyoto University, for their valuable help. We also thank Hirohiko Nakano of Ritsumeikan University, for valuable discussion. This work was supported in part by a Grant-in-Aid for Scientific Research by the Japanese Ministry of Education.

[1]R. A. Ferrell, Phys. Rev. **108**, 167 (1957).

[2]J. L. Levine and T. M. Sanders, Jr., Phys. Rev. **154**, 138 (1967).

[3]H. R. Harrison, L. M. Sander, and B. E. Springett, J. Phys. B **6**, 908 (1973).

[4]J. A. Jahnke, M. Silver, and J. P. Hernandez, Phys. Rev. B **12**, 3420 (1975).

[5]L. O. Roellig and T. M. Kelly, Phys. Rev. Lett. **18**, 387 (1967).

[6]K. F. Canter, J. D. McNutt, and L. O. Roellig, Phys. Rev. A **12**, 375 (1975).

[7]J. B. Smith, Jr., J. D. McGervey, and A. J. Dahm, Phys. Rev. B **15**, 1378 (1977).

[8]K. Rytsölä, J. Vettenranta, and P. Hautojärvi, J. Phys. B **17**, 3359 (1984).

[9]R. M. Nieminen, I. Välimaa, M. Manninen, and P. Hautojärvi, Phys. Rev. A **21**, 1677 (1980).

[10]J. P. Hernandez, Phys. Rev. A **14**, 1579 (1976).

[11]I. T. Iakubov and A. G. Khrapak, Appl. Phys. **16**, 179 (1978).

[12]M. Tuomisaari, K. Rytsölä, R. M. Nieminen, and P. Hautojärvi, J. Phys. B **19**, 2667 (1986).

[13]M. J. Stott and E. Zaremba, Phys. Rev. Lett. **38**, 1493 (1977).

[14]M. Manninen and P. Hautojärvi, Phys. Rev. B **17**, 2129 (1978).

[15]M. Tuomisaari, K. Rytsölä, and P. Hautojärvi, Phys. Lett. **112A**, 279 (1985).

[16]K. Rytsölä, K. Rantapuska, and P. Hautojärvi, J. Phys. B **17**, 299 (1984).

[17]J. P. Hernandez, Phys. Rev. B **11**, 1289 (1975).

[18]C. Ebner and C. Punyanitya, Phys. Rev. A **19**, 856 (1979).

[19]A. G. Khrapak and I. T. Iakubov, Zh. Eksp. Teor. Fiz. **69**, 2042 (1975) [Sov. Phys.—JETP **42**, 1036 (1976)].

[20]R. L. Moore, C. L. Cleveland, and H. A. Gersch, Phys. Rev. B **18**, 1183 (1978).

[21]J. D. McNutt and S. C. Sharma, J. Chem. Phys. **68**, 130 (1978).

[22]S. C. Sharma, J. D. McNutt, A. Eftekhari, and R. A. Hejl, J. Chem. Phys. **75**, 1226 (1981).

[23]S. C. Sharma, A. Eftekhari, and J. D. McNutt, Phys. Rev. Lett. **48**, 953 (1982).

[24]G. L. Wright, M. Charlton, G. Clark, T. C. Griffith, and G. R. Heyland, J. Phys. B **16**, 4065 (1983).

[25]T. Kawaratani, Y. Nakayama, and T. Mizogawa, Phys. Lett. **108A**, 75 (1985).

[26]T. P. Eggarter and M. H. Cohen, Phys. Rev. Lett. **25**, 807 (1970); **27**, 129 (1971).

[27]T. P. Eggarter, Phys. Rev. A **5**, 2496 (1972).

[28]J. P. Hernandez, J. Phys. C **15**, 1923 (1982).

[29]D. W. Smith and J. P. Hernandez, J. Chem. Phys. **77**, 5802 (1982).

[30]E. O. Kane, Phys. Rev. **131**, 79 (1963).

[31]R. T. Jacobsen, R. B. Stewart, R. D. McCarty, and H. J. M. Hanley, *Thermophysical Properties of Nitrogen from the Fusion Line to 3500R for Pressures to 150,000 PSIA,* Natl. Bur. Stand. Tech. Note **648** (1973).

[32]A. L. Gosman, R. D. McCarty, and J. G. Hurst, *Thermodynamic Properties of Argon from the Triple Point to 300 K at Pressures to 1000 atmospheres,* Natl. Bur. Stand. Ref. Data Series, Natl. Bur. Stand. (U.S.) NSRDS-NBS**27**(U.S. GPO, Washington, D.C., 1969), Vol. 27.

[33]P. G. Coleman, T. C. Griffith, G. R. Heyland, and T. L. Killeen, Appl. Phys. **3**, 271 (1974).

[34]P. G. Coleman, T. C. Griffith, and G. R. Heyland, Appl. Phys. **5**, 223 (1974).

[35]D. W. Gidley, A. Rich, P. W. Zitzewitz, and D. A. L. Paul, Phys. Rev. Lett. **40**, 737 (1978).

[36]K. F. Caswell and G. P. Lepage, Phys. Rev. A **20**, 36 (1979).

[37]T. C. Griffith and G. R. Heyland, Phys. Rep. **39**, 169 (1978).

[38]J. D. McNutt, V. B. Summerour, A. D. Ray, and P. H. Huang, J. Chem. Phys. **62**, 1777 (1975).

[39]R. A. Fox, K. F. Canter, and M. Fishbein, Phys. Rev. A **15**, 1340 (1977).

[40]J. D. McNutt, S. C. Sharma, M. H. Franklin, and M. A. Woodall II, Phys. Rev. A **20**, 357 (1979).

[41]The previous results of ${}^1Z_{\text{eff}}$ and D^* in Ref. 25 are incorrect due to an error in the computer program. The value of ${}^1Z_{\text{eff}}$ for the combined data of the linear regions at all four temperatures is changed to 0.252 ± 0.001.

[42]M. Benedict, G. B. Webb, and L. C. Rubin, Chem. Eng. Prog. **47**, 419 (1951).

[43]D. B. Mann, *Thermodynamic Properties of Helium from 6 to 540R between 10 and 1500 PSIA,* Natl. Bur. Stand. Tech. Note **154A** (1962).

[44]In the pressure ranges corresponding to the data, for example, with the density $D<1.5D^*$, the slopes are 57.2 ± 0.3, 57.3 ± 0.4, 57.4 ± 0.4, and 57.7 ± 0.2 at 100, 120, 130, and 170 K, respectively.

[45]P. K. Tseng, S. Y. Chuang, S. H. Chen, and S. J. Tao, in *Proceedings of the 5th International Conference on Positron Annihilation, Lake Yamanaka, Japan, 1979,* edited by R. R. Hasiguti and K. Fujiwara (Japan Institute of Metals, Sendai, 1979), p. 557.

[46]J. Jortner, N. R. Kestner, S. A. Rice, and M. H. Cohen, J. Chem. Phys. **43**, 2614 (1965).

[47]J. R. Broomall, W. D. Johnson, and D. G. Onn, Phys. Rev. B **14**, 2819 (1976).

[48]M. J. Stott and P. Kubica, Phys. Rev. B **11**, 1 (1975); M. J. Stott and R. N. West, J. Phys. F **8**, 635 (1978).

[49]The linear relations obtained by weighted least-squares fits are

$(0.18\pm0.03)(D-D_I)+(0.04\pm0.06)$, $(0.20\pm0.01)(D-D_I)+(0.02\pm0.04)$, $(0.19\pm0.01)(D-D_I)+(0.02\pm0.03)$, and $(0.20\pm0.02)(D-D_I)+(-0.04\pm0.08)$ at 100, 120, 130, and 170 K, respectively.

[50]H. L. Frisch, J. M. Hammersley, and D. J. A. Welsh, Phys. Rev. **126**, 949 (1962).
[51]J. P. Hernandez, Phys. Rev. A **5**, 635 (1972).